https://doi.org/10.1103/PhysRevMaterials.4.084603

Insight into the electronic structure of semiconducting ϵ-GaSe and ϵ-InSe

S. V. Eremeev[1,2,3], M. Papagno[4], I. Grimaldi[4], O. De Luca[4], L. Ferrari[5], Asish K. Kundu[6], P. M. Sheverdyaeva[6], P. Moras[6], G. Avvisati[7], A. Crepaldi[8], H. Berger[8], I. Vobornick[9], M. G. Betti[7], M. Grioni[8], C. Carbone[6], E. V. Chulkov[3,10,11], and D. Pacilé[4*]

[1] *Institute of Strength Physics and Materials Science, 634055, Tomsk, Russia*
[2] *Tomsk State University, 634050, Tomsk, Russia*
[3] *Saint Petersburg State University, Saint Petersburg, 198504, Russia*
[4] *Dipartimento di Fisica, Università della Calabria, 87036 Arcavacata di Rende (CS), Italy*
[5] *Istituto di Struttura della Materia, Consiglio Nazionale delle Ricerche, Roma, Italy*
[6] *Istituto di Struttura della Materia, Consiglio Nazionale delle Ricerche, Trieste, Italy*
[7] *Dipartimento di Fisica, Università di Roma "La Sapienza", I-00185 Roma, Italy*
[8] *Insitute of Physics, Ecole Polytechnique Fédérale de Lausanne (EPFL), CH-1015 Lausanne, Switzerland*
[9] *Istituto Officina dei Materiali (IOM)-CNR, Laboratorio TASC, Area Science Park, S.S.14, Km 163.5, 34149 Trieste, Italy*
[10] *Donostia International Physics Center (DIPC), 20018 San Sebastin/Donostia, 20080, Basque Country, Spain*
[11] *Departamento de Fisica de Materiales UPV/EHU, Centro de Fisica de Materiales CFM MPC and Centro Mixto*

Metal mono-chalcogenides (MX) have recently been rediscovered as two-dimensional (2D) materials with electronic properties highly dependent on the number of layers. Although some intriguing properties appear in the few-layer regime, the carrier mobility of MX compounds increases with the number of layers, motivating the interest in multi-layered hetero-structures or bulk materials. By means of angle-resolved photoemission spectroscopy (ARPES) measurements and density functional theory (DFT) calculations, we compare the electronic band structure of bulk ϵ-GaSe and ϵ-InSe semiconductors. We focus our attention on the top valence band of the two compounds along main symmetry directions, discussing the effect of spin-orbit coupling and contributions from post-transition metal (Ga or In) and Se atoms. Our results show that the top valence band at Γ-point is dominated by Se p_z states, while the main effect of Ga or In appears more deeply in binding energy, at the Brillouin zone corners, and in the conduction band. This findings explain also the experimental observation of a hole effective mass rather insensitive to the post-transition metal. Finally, by means of spin-resolved ARPES and surface band structure calculations we describe Rashba-Bychkov spin splitting of surface states in ϵ-InSe.

I. INTRODUCTION

The electronic properties of layered mono-chalcogenides (MX, where M stands for the post-transition metal, and X represents the chalcogen atom), among them GaSe and InSe, have recently been the focus of extensive research, mainly devoted to the discovery of unique properties in the few-layers regime [1–6]. MX compounds exhibit a direct band gap in the bulk (GaSe of about 2.0 eV [7] and InSe of about 1.3 eV [8] at room temperature (RT)), while they acquire an indirect band gap for few layers. Films of different thickness exhibit variable width of the band gap, thus they are optically active in the IR and visible region and are tested as active components in photodetectors [3, 9, 10]. Moreover, vertical van der Waals (vdW) heterostructures obtained by combining different two-dimensional (2D) materials have been investigated in order to create novel functionalities [11–15], or to increase the carrier mobility [8, 16].

The possibility to manipulate vertical vdW heterostructures requires a detailed knowledge of single components, starting from the bulk counterpart down to a single-layer. Through angle-resolved photoemission spectroscopy (ARPES) measurements and density functional theory (DFT) calculations, the present study aims at clarifying the role of the metal and Se chalcogenides atoms in the bulk electronic structure of two related MX compounds, ϵ-GaSe and ϵ-InSe. The single tetra-layer of each compound consists of four covalently bonded Se-M-M-Se atoms (M stands for Ga or In), while different tetra-layers are held together by vdW forces, making the compounds easily exfoliable. For each MX compound there are different polytypes (ϵ-MSe, β-MSe, γ-MSe, δ-MSe)[17, 18], which differ in the symmetry and structure of the crystal lattice, and present specific physical properties [19]. The bulk ϵ polytype (Fig. 1 (a)) is made up by superposition of a pair of tetralayers with AB stacking. It belongs to the $P\bar{6}/m2$ non-centrosymmetric space group ($D^1{}_{3h}$), regardless of the number of layers.

It has been widely shown that both ϵ-GaSe and ϵ-InSe have band edges located at Γ in the bulk structure [11, 12], while decreasing the number of layers the valence band maximum (VBM) slightly shifts away from Γ, creating a bow-shaped valence band, often called inverted "Mexican hat" [20]. The band structure in the few-layers regime has attracted most of the attention as the peculiar shape yields high density of states (DOS) and Van Hove singularity near the VBM, leading to unconventional correlation effects [21]. Concerning bulk GaSe and InSe, it has been shown that spin-orbit interaction of MX

*E-mail address: daniela.pacile@fis.unical.it

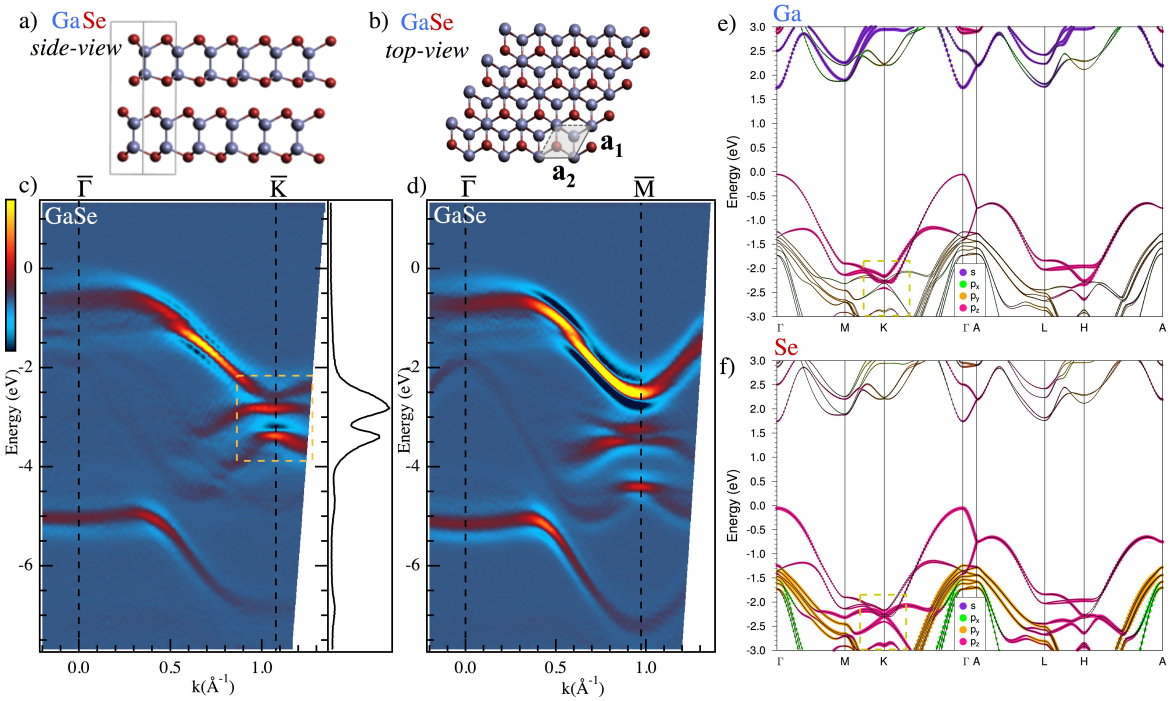

FIG. 1: (Color online) Sketch of the ϵ-GaSe crystal structure: (a) side-view; (b) top-view. Experimental band structure, shown in second derivative, along $\bar{\Gamma}$-$\bar{K}$ (c) and $\bar{\Gamma}$-$\bar{M}$ (d), taken with photon energy of 45 eV. On the right side of panel (c), the energy distribution curve extracted from raw data at $\bar{K}$-point is reported. (e,f) Calculated orbital-projected bulk band structure along high-symmetry directions of hexagonal Brillouin zone with weights of Ga (e) and Se (f) orbitals, where sizes of the circles are proportional to the contribution of the corresponding orbitals.

compounds lifts band degeneracies, causing a splitting of several hundreds meV just below the VBM, and yielding measurable differences in high-energy photoluminescence transition energies [11, 12].

Since the first days of discovery of these semiconductors [22], the high carrier mobility and its physical mechanism have been the subject of discussion between different authors [23–25]. The understanding of these properties requires a wide-spectrum information on the electronic band structure. Our ARPES and DFT study of ϵ-GaSe and ϵ-InSe sheds light on the atomic contributions to the conduction and valence band. We show that the post-transition metal has a key role in tuning the energy position of the conduction band minimum (CBM) and the energy width of the band gap, leaving unaffected the shape of top valence band. Spin-ARPES measurements of ϵ-InSe show Rashba-Bychkov spin splitting of localized surface states. The description of our results has involved a carefully comparison with different theoretical approaches.

II. METHODS

Single crystalline ingots of GaSe and InSe were grown in double wall ampoules by means of the Bridgman method starting from a nonstoichiometric melt, containing an In excess of about 5% [26]. The high quality of the as-grown ingots, as well as the structural phase (ϵ polytype) of InSe was proved by using X-ray diffraction (XRD), transmission electron microscopy (TEM) and Raman spectroscopy, and reported elsewhere [27]. The XRD characterization of ϵ-GaSe is instead reported in the Supplemental Material (Fig. S1). Photoemission measurements were performed on fresh surfaces obtained by cleavage at RT in ultrahigh-vacuum (UHV) conditions. The high quality of the achieved (111) surfaces was verified by sharp features in the low-energy electron diffraction (LEED) pattern, reported in the Supplemental Material (Fig. S2). The ARPES measurements were performed at the VUV Photoemission beamline of the Elettra synchrotron, with the sample kept at 18 K, using a Scienta R−4000 hemisferical electron analyzer, which allows parallel acquisition over 30° angular range. The energy and angular resolution of ARPES were set to 15 meV and 0.3 degrees, respectively. Spin-resolved ARPES measurements were performed at the APE beamline of the Elettra synchrotron by use of a very low-energy electron diffraction (VLEED)-based spin polarimeter [28]. Energy and angular resolution were set to 100 meV and 1.0 degree.

All ARPES spectra have been aligned to the VBM for an easier comparison with the theoretical band structure.

The density functional theory calculations were performed by using the Vienna Ab initio Simulation Package (VASP) [29, 30], with core electrons rep-

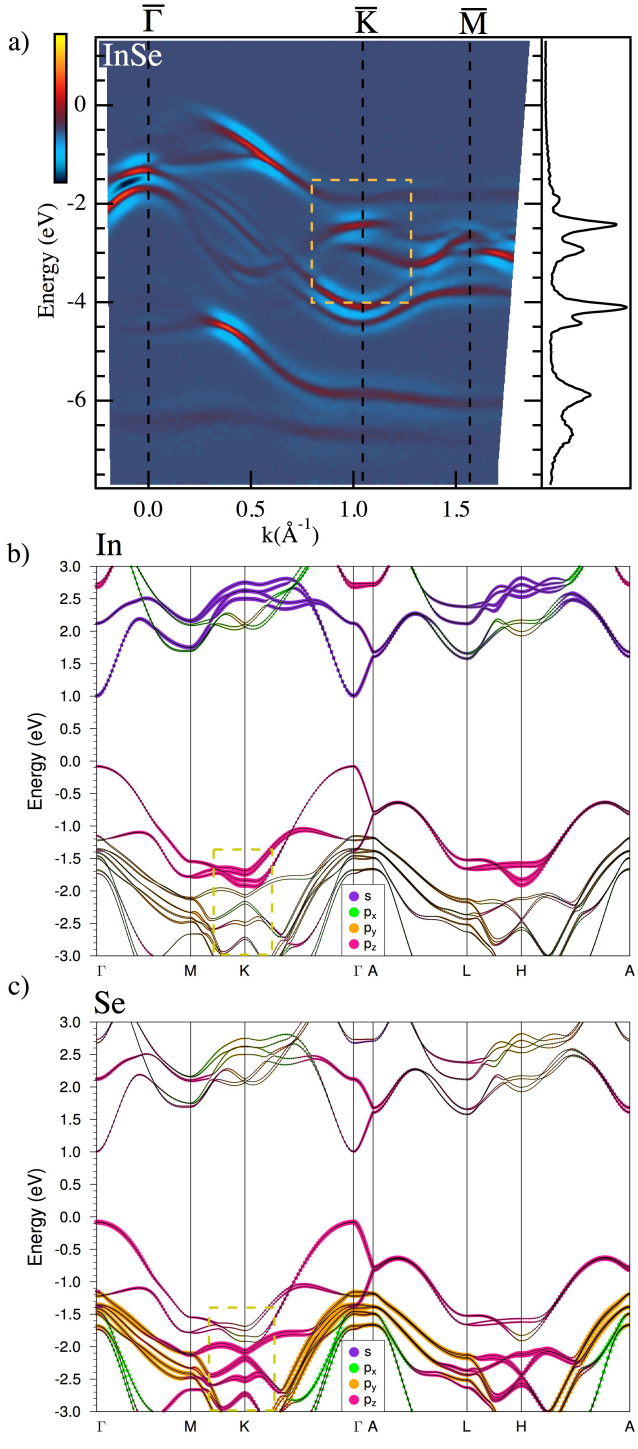

FIG. 2: (Color online) (a) Experimental band structure of ϵ-InSe, shown in second derivative along $\bar{\Gamma}\bar{K}\bar{M}$, taken with photon energy of 65 eV. On the right side, the energy distribution curve extracted from raw data at $\bar{K}$-point is reported. (b,c) The same as in Fig. 1 (e,f) but for In and Se orbitals.

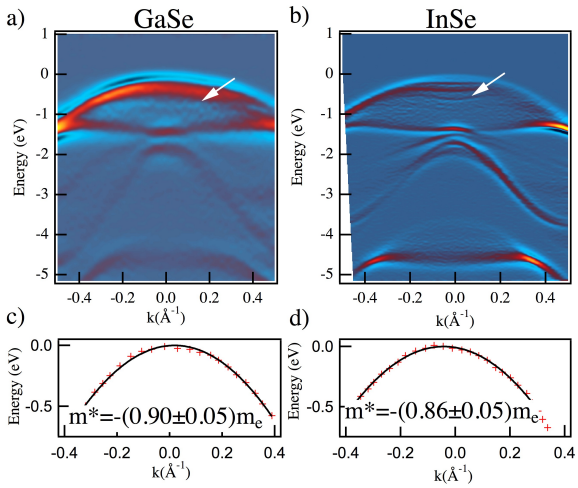

FIG. 3: (Color online) Experimental band structure of ϵ-GaSe (a) and ϵ-InSe (b), shown in second derivative, taken along the $\bar{M}$-$\bar{\Gamma}$-$\bar{M}$ high symmetry axis (photon energy is 40 eV). (c-d) Determination of the hole effective mass through a parabolic model from the experimental dispersion (red crosses) extracted from the top band in (a) and (b), respectively.

resented by projector augmented wave (PAW) potentials [31, 32]. For bulk parameters optimization the generalized gradient approximation (GGA-PBE) [33] to the exchange-correlation potential and DFT-D3 van der Waals correction [34] were applied. The equilibrium lattice parameters of GaSe(InSe) a=3.778(4.041)Å, c=15.943(16.723)Å are in fine agreement with experimental data, a=3.757(±0.015)Å and c=15.998(±0.032)Å for GaSe, as extracted from Fig. S1, and a=4.005(±0.022)Å and c=16.672(±0.045)Å for InSe [27]. However, the bulk gaps obtained within GGA-PBE calculations are much smaller than the experimental values. They are 0.795 eV for GaSe and 0.315 eV for InSe. To obtain more accurate bulk band structures, the modified Becke-Johnson (mBJ) exchange potential [35, 36], which has been shown to be the most accurate semilocal potential for band gap calculations was adopted. The mBJ bulk gaps of 1.801 and 1.087 eV for GaSe and InSe, respectively, are in satisfactory agreement with the experiments. We also have done the calculations using HSE06 screened hybrid functional. [37] The HSE06 bulk gaps are 1.635 and 1.034 eV for GaSe and InSe, respectively. Spin-orbit interaction (SOI) was included in all types of calculations.

For surface band structure calculations we use slabs of 56 atomic layers thickness (14 tetra-layers) which were relaxed within GGA-PBE approach with DFT-D3 van der Waals correction included. Atoms of two tetra-layers on both sides of the slab were allowed to relax whereas the atoms in the internal layers were fixed to their equilibrium bulk positions.

III. RESULTS AND DISCUSSION

The electronic band structure of ϵ-GaSe and ϵ-InSe was investigated using ARPES and DFT calculations. According to the hexagonal surface symmetry (Fig. 1 (b)), an insight in the electronic structure requires the investigation of the band dispersion along two symmetry directions. In Fig. 1 (c-d) we report the GaSe bulk band structure projection on the surface Brillouin zone (BZ) along the $\bar{\Gamma}$-$\bar{\mathrm{K}}$ and $\bar{\Gamma}$-$\bar{\mathrm{M}}$ directions, taken with photon energy of 45 eV and shown in second derivative. The topmost part of the valence band is found at $\bar{\Gamma}$-point, down-dispersing along both high-symmetry directions. In Fig. 1 (e-f) we show the GaSe calculated bands projected on Ga and Se orbitals, respectively. Our simulation proves that for a bulk system the VBM is located at Γ, and both systems do have a direct band, in agreement with earlier results [1, 4]. By inspection of theoretical results, we prove that the top valence band of bulk GaSe has a dominant p_z component of both Ga and Se atoms (pink circles in Fig. 1 (e-f)), with about two times higher weight of Se atoms. Moreover, below about 1 eV from the VBM, mainly p_y and p_x components of Se atoms (yellow and green circles in Fig. 1 (f), respectively) are present. Similar results are obtained for bulk InSe, as reported in Fig. 2 (b-c). Comparing the two compounds, we deduce that Se p_z states are expected to dominate at the VBM, thus a different group III-metal does not change significantly the outer occupied states of the semiconductor. ARPES measurements of ϵ-GaSe reported in Fig. 1(c-d) and ϵ-InSe in Fig. 2 (a) display similar top valence bands, supporting the theoretical findings. Moreover, the highest bands with dominant p_z component exhibit a similar slop along the $\bar{\Gamma}$-$\bar{\mathrm{K}}$ direction, and reach the $\bar{\mathrm{K}}$-point almost flat, due to a reduced and similar length of the c^* reciprocal lattice parameter. Contrarily, lower lying bands with their maximum at about -1.5 eV at $\bar{\Gamma}$-point, which have dominant p_x and p_y components, as described by our theoretical calculations (yellow and green circles in Fig. 1 (f) and Fig. 2 (c)), exhibit a different slope along $\bar{\Gamma}$-$\bar{\mathrm{K}}$. This slope is indeed more pronounced for ϵ-GaSe, which have a slightly higher (of about 7%) a^* reciprocal lattice parameter with respect to ϵ-InSe.

The bottom of the conduction band, instead, is mainly due to Ga (In) s states, thus more sensitive to the post-transition metal. On the other hand, from a closer look at the color scale of the occupied bands in Fig. 1 (e-f) and Fig. 2 (b-c), one can see that the p_z weight of Ga/In is prevailing near the corners of BZ, that is at K(H) points. This predicted difference is clearly seen in Fig. 1c and Fig. 2a at the $\bar{\mathrm{K}}$-point, as highlighted by dashed yellow lines and energy distribution curves reported on the corresponding right panels. We point out that, the two top-most surface projected bands of ϵ-GaSe overlap at $\bar{\mathrm{K}}$-point (Fig. 1c), while they are clearly separated by about 0.50 eV for ϵ-InSe (Fig. 2a). The agreement with our simulations along surface symmetry directions, and specifically at the $\bar{\mathrm{K}}$-point, is further supported by projected band structure calculations reported in the Supplemental Material (Fig. S3). Here, at the $\bar{\mathrm{K}}$-point, the spin-orbit splitting of the topmost band is almost twice larger in InSe (71 meV) as compared to GaSe (40 meV). However, the magnitude of the splitting in both cases is smaller with respect to k_z dispersion of the bands, and this hampers its detection by photoemission.

We further discuss the comparison between the two compounds by focussing on the VBM. The parabolic shape of the VBM close to Γ in bulk GaSe and InSe results from the close proximity of multiple subbands [16], originating from the interlayer coupling and decreasing in number in the few-layers regime, up to the unique inverted sombrero-like band of a single tetra-layer. These narrowly spaced subbands are clearly visible in our measurements, due to the high quality of the crystal samples. In Fig. 3 (a-b) we report the band structure of GaSe and InSe, respectively, along the $\bar{\mathrm{M}}$-$\bar{\Gamma}$-$\bar{\mathrm{M}}$ high symmetry axis, where we highlight by white arrows multiple subbands. From the topmost energy distribution curves we estimate the corresponding hole effective mass (Fig. 3 (c-d)) obtaining values close to m_e for both compounds, in agreement with previous results reported for InSe[12]. The comparable hole effective mass of GaSe and InSe provides additional evidence of the dominant Se p_z character of the top valence band.

In order to detect the effect of spin orbit interaction on the surface electronic structure, we have acquired spin-resolved ARPES measurements for ϵ-InSe (Fig. 4). The measurements were performed at 35 eV of photon energy using linearly p-polarised light. Spin-polarization data were discerned only in the experimental geometry parallel to the plane of incidence. Considering that the APE DA30 momentum dispersion plane is perpendicular to the Elettra orbit, in this geometry the in-plane spin component (along k_y) perpendicular to the selected high symmetry direction (along k_x) was probed. Corresponding spin-resolved EDCs, shown at k_x= (-0.37±0.05)Å^{-1} and k_x= (0.37±0.05)Å^{-1} (top-left and top-right panels of Fig. 4, respectively) exhibit a considerable spin polarization. Moreover, the spin polarization reverses upon changing the sign of k_x (b, c and d peaks, located at about 3.6 eV, 3.4 eV and 3.2 eV from the VBM, respectively) and it vanishes at k_x=0 (data not shown). This observed Rashba-Bychkov type spin polarization has been explored by means of surface band structure calculations.

First, we compared the valence band calculated within GGA-PBE, HSE06, and mBJ approaches with experimental spectrum. Despite its failure to reproduce the band gap, GGA-PBE describes better the experimental valence band compared to the other two. The total width of the measured VB at the $\bar{\Gamma}$ point amounts about 4.5 eV (Fig. 4, center panel). In particular, as can be seen in Fig. 5 (a), the deep band, which is mainly composed by In s orbitals, hybridized with p_z Se orbitals is very sensitive to the exchange-correlation functional. The GGA-PBE nicely reproduces the experimental VB width whereas

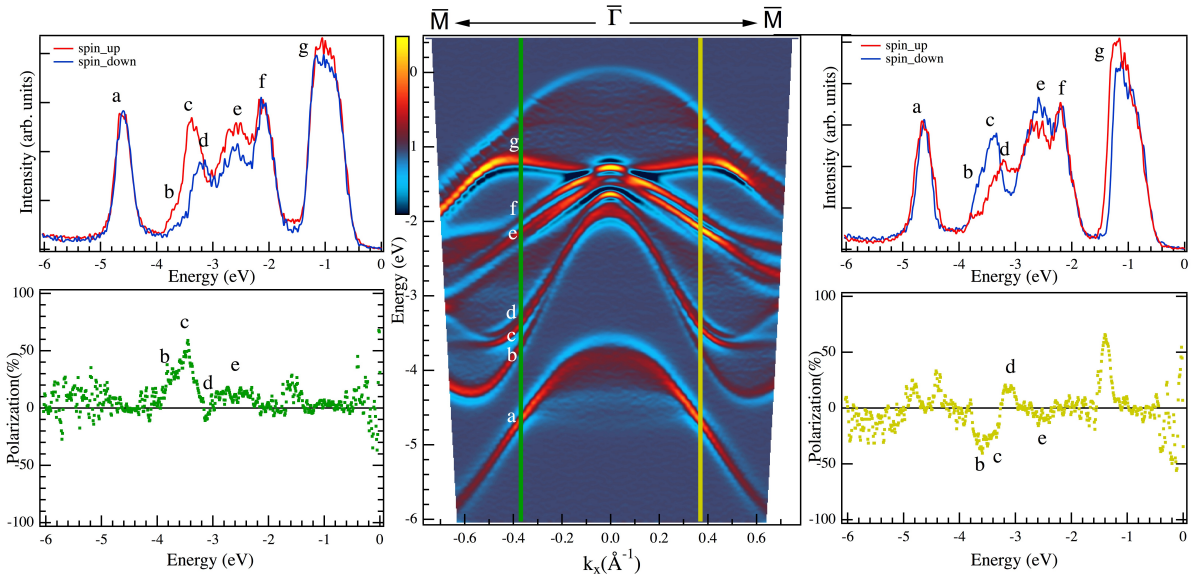

FIG. 4: (Color online) Spin-ARPES data of ϵ-InSe: (central panel) experimental band structure shown in second derivative along the $\bar{M}$-$\bar{\Gamma}$-$\bar{M}$ high symmetry axis (photon energy is 35 eV using linearly p-polarised light); (left-right panels) spin-resolved curves and corresponding spin polarization showing the spin texture of selected bands indicated by green and yellow lines in the central panel.

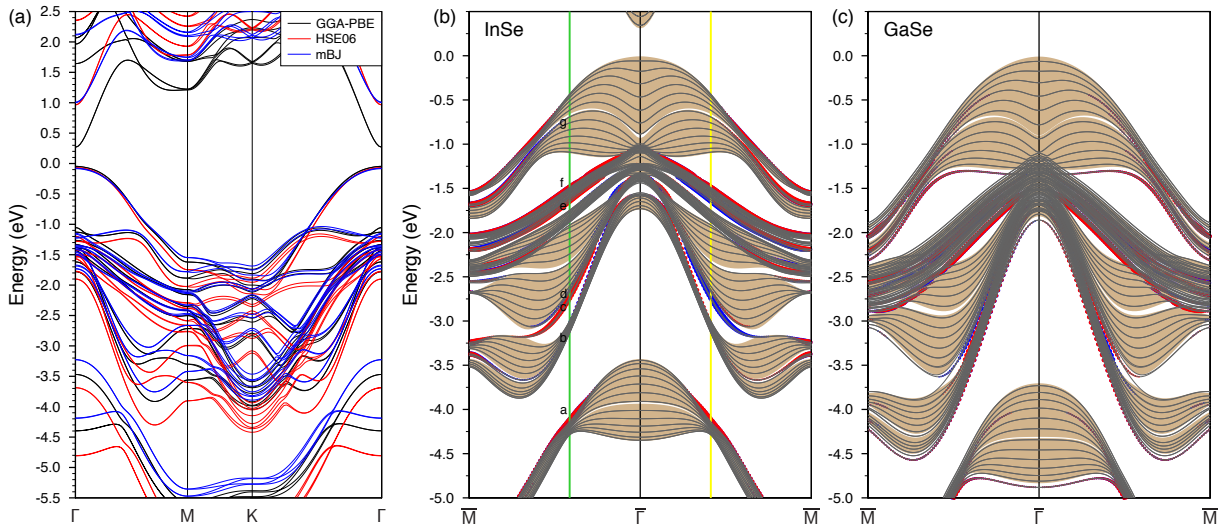

FIG. 5: (Color online) Bulk band structure of InSe as calculated within GGA-PBE, HSE06, and mBJ approaches (a). Calculated surface electronic structure and spin polarization of InSe (b) and GaSe (c). Red/blue circles represent positive/negative sign of the in-plane spin component for the surface states. Shaded areas correspond to projection of the bulk states on the (111) plane. Green and yellow vertical lines in panel (a) mark $k_{\|}$ where the spin polarization was measured, see Fig. 4 (central panel).

HSE06(mBJ) noticeably overestimate(underestimate) it. The same behavior is observed for GaSe. For this reason we have done surface band structure calculations within the GGA-PBE approach. Fig. 5 (b) shows the surface spectrum of InSe. Even if, whereas the fundamental band gap is free of surface states, the valence band hosts several localized states which are experiencing the Rashba spin splitting. However, this splitting in general is negligible (red and blue circles in Fig. 5 (b) are noticeably overlapped) with exception of several states which are split off from the edge of the bulk states more than others. For instance, the state located inside the local VB gap which crosses experimental k_x green/yellow lines at about -2.7 eV and whose spin counterpart merges with bulk states, can be confidently identified with the highly spin polarized experimental peak c even if about 0.6 eV higher in energy. As for other experimental peaks which demonstrate significantly weaker spin polarization or do not show it at all, the corresponding slightly split bands can also be found in the calculated spectrum at energies of about 0.5-0.8 eV higher compared to experimental values. The variable difference between calculated and experimental energies is due to a reduced split off between surface states and bulk bands, which would require similar accuracy in their simulation, as well as in their detection. We notice also that the polarization sign of c,d and e peaks of Fig. 4 is well described by our surface band structure calculations, while the splitting of b peak is barely visible within bulk states in Fig. 5. The Rashba splitting in the surface states of GaSe (Fig. 5 (c)) is even less pronounced as compared with InSe and can hardly be detected experimentally.

IV. CONCLUSIONS

We compare the experimental band structure of two promising MX compounds, ϵ-GaSe and ϵ-InSe. We show that the VBM is dominated by Se atoms, as proved by ARPES data of the top valence band, a comparable hole effective mass, and confirmed by calculations of orbital-projected bulk band structure. The predicted CBM, instead, is more influenced by the post-transition metals. Our description supports a major influence of the conduction band in affecting the electronic properties of related MX compounds. We also compare the valence band calculated within GGA-PBE, HSE06, and mBJ approaches with experimental data, showing limitations in describing band gap and valence band deep. Finally, within the GGA-PBE approach, we describe the measured Rashba splitting in the surface states of ϵ-InSe.

Acknowledgements

The support by the Fundamental Research Program of the State Academies of Sciences (line of research III.23.2.9), and the project EUROFEL-ROADMAP ESFRI, are gratefully acknowledged. M. Castriota and F. Ciuchi, from Università della Calabria (Italy), are acknowledged for having performed, respectively, Raman and XRD characterization of GaSe and InSe samples. The authors acknowledge support from the Saint Petersburg State University (Grant No. 51126047).

[1] Z. Ben Aziza, V. Zólyomi, H. Henck, D. Pierucci, M. G. Silly, J. Avila, S. J. Magorrian, J. Chaste, C. Chen, M. Yoon *et al.*, Phys. Rev. B **98**, 115405 (2018).
[2] A. Azizi, G. Antonius, E. Regan, R. Eskandari, S. Kahn, F. Wang, S. G. Louie and A. Zettl, Nano Lett. **19**, 3, 1782-1787 (2019).
[3] P. Li and I. Appelbaum, Phys. Rev. B **92**, 195129 (2015).
[4] X. Li, M. W. Lin, A. A. Puretzky, J. C. Idrobo, C. Ma, M. Chi, M. Yoon, C. M. Rouleau, I. I. Kravchenko, D. B. Geohegan and K. Xiao, Sci. Rep. **4**, 5497 (2014).
[5] D. V. Rybkovskiy, N. R. Arutyunyan, A. S. Orekhov, I. A. Gromchenko, I. V. Vorobiev, A. V. Osadchy, E. Yu. Salaev, T. K. Baykara, K. R. Allakhverdiev, and E. D. Obraztsova, Phys. Rev. B **84**, 085314 (2011).
[6] M. W. Chen, H. Kim, D. Ovchinnikov, A. Kuc, T. Heine, O. Renault, and A. Kis, npj 2D Mater. Appl., **2**, 2 (2018).
[7] D. J. Terry, V. Zólyomi, M. Hamer, A. V. Tyurnina, D. G. Hopkinson, A. M. Rakowski, S. J. Magorrian, N. Clark, Y. M. Andreev, O. Kazakova *et al.*, 2D Mater. **5**, 041009 (2018).
[8] D. A. Bandurin, A. V. Tyurnina, G. L. Yu, A. Mishchenko, V. Zólyomi, S. V. Morozov, R. K. Kumar, R. V. Gorbachev, Z. R. Kudrynskyi, S. Pezzini, Z. D. Kovalyuk *et al.*, Nat. Nanotechnol. **12**, 223-227 (2017).
[9] T. Wang, J. Li, Q. Zhao, Z. Yin, Y. Zhang, B. Chen, Y. Xie and W. Jie, Materials **11**, 2, 186 (2018).
[10] P. Hu, Z. Wen, L. Wang, P. Tan and K. Xiao, ACS Nano **6**, 7, 5988-5994 (2012).
[11] Z. Ben Aziza, H. Henck, D. Pierucci, M. G. Silly, E. Lhuillier, G. Patriarche, F. Sirotti, M. Eddrief and A. Ouerghi, ACS Nano **10**, 10, 9679-9686 (2016).
[12] H. Henck, D. Pierucci, J. Zribi, F. Bisti, E. Papalazarou, J.-C. Girard, J. Chaste, F. Bertran, P. Le Fre, F. Sirotti *et al.*, Phys. Rev. Materials **3**, 034004 (2019).
[13] Z. Ben Aziza, D. Pierucci, H. Henck, M. G. Silly, C. David, M. Yoon, F. Sirotti, K. Xiao, M. Eddrief, J.-C. Girard and A. Ouerghi, Phys. Rev. B **96**, 035407 (2017).
[14] C. H. Lee, S. Krishnamoorthy, D. J. O′Hara, M. R. Brenner, J. M. Johnson, J. S. Jamison, R. C. Myers, R. K. Kawakami, J. Hwang, and S. Rajan, J. Appl. Phys. **121**, 094302 (2017).
[15] F. Yan, L. Zhao, A. Patanè, P. Hu, X. Wei, W. Luo, D. Zhang, Q. Lv, Q. Feng, C. Shen *et al.*, Nanotechnology **28**, 27, 27LT01 (2017).
[16] W. Li, S. Poncé, and F. Giustino, Nano Lett. **19**, 1774-1781 (2019).
[17] R. Longuinhos and J. Ribeiro-Soares, Phys. Chem. Chem. Phys. **18**, 25401-25408 (2016).
[18] N. C. Fernelius, Prog. Crystal Growth and Charact. **28**, 275-353 (1994).

[19] J. Srour, M. Badawi, F. E. H. Hassan, and A. Postnikov, J. Chem. Phys. **149**, 054106 (2018).
[20] M. J. Hamer, J. Zultak, A. V. Tyurnina, V. Zólyomi, D. Terry, A. Barinov, A. Garner, J. Donoghue, A. P. Rooney, V. Kandyba *et al.*, ACS Nano **13**, 2, 2136-2142 (2019).
[21] T. Cao, Z. Li, and S. G. Louie, Phys. Rev. Lett. **114**, 236602 (2015).
[22] R. Fivaz and E. Mooser, Phys. Rev. B **163**, 743 (1967).
[23] S. Sucharitakul, N. J. Goble, U. R. Kumar, R. Sankar, Z. A. Bogorad, F.-C. Chou, Y.-T. Chen, and X. P. A. Gao, Nano Lett. **15**, 6, 3815-3819 (2015).
[24] A. Sh. Abdinov, R. F. Babaeva, N. A. Ragimova, R. M. Rzaev, and S. I. Amirova, Inorg. Mater. **50** (4), 334-338, (2014).
[25] A. Segura, F. Pomer, A. Cantarero, W. Krause, and A. Chevy, Phys. Rev. B **29**, 5708 (1984).
[26] A. Chevy, A. Khun, and S. Martin, Journal of Crystal Growth **38**, 1, 118-122 (1977).
[27] I. Grimaldi, T. Gerace, M. M. Pipita, I. D. Perrotta, F. Ciuchi, H. Berger, M. Papagno, M. Castriota, and D. Pacilè, Solid State Comm. **311**, 113855 (2020).
[28] C. Bigi, P.K. Das, D. Benedetti, F. Salvador, D. Krizmancic, R. Sergo, A. Martin, G. Panaccione, G. Rossi, J. Fujii, I. Vobornik, J. Synchrotron Radiat. **24**, 750-756 (2017).
[29] G. Kresse and J. Hafner, Phys. Rev. B **48**, 13115 (1993).
[30] G. Kresse, J. Furthmüller, Phys. Rev. B **54**, 11169 (1996).
[31] P.E. Blöchl, Phys. Rev. B **50**, 17953 (1994).
[32] G. Kresse, D. Joubert, Phys. Rev. B **59**, 1758 (1999).
[33] J.P. Perdew, K. Burke, M. Ernzerhof, Phys. Rev. Lett. **77**, 3865 (1996).
[34] S. Grimme, J. Antony, S. Ehrlich, and H. Krieg, J. Chem. Phys. **132**, 154104 (2010).
[35] A. D. Becke and E. R. Johnson, J. Chem. Phys. **124**, 221101 (2006).
[36] F. Tran and P. Blaha, Phys. Rev. Lett. **102**, 226401 (2009).
[37] A.V. Krukau, O.A. Vydrov, A.F. Izmaylov, and G.E. Scuseria, J. Chem. Phys. **125**, 224106 (2006).